ACS OMEGA

Open Access

http://pubs.acs.org/journal/acsodf

Article

Receptor-Selective Modulation of Cannabinoid Signaling by Cardamonin: Integrating Molecular Dynamics, Free Energy Calculations, and Behavioral Validation

Mohamed Hanief Khalid,[#] Liyana Azmi,[#] M. Qadri E. Mubarak,[#] Nur Mazniatul Iqma Marsujak, Amir Syahir, Enoch Kumar Perimal, Mohd Roslan Sulaiman, and Muhamad Arif Mohamad Jamali*

Cite This: *ACS Omega* 2026, 11, 23820−23832

Read Online

ACCESS | Metrics & More | Article Recommendations | Supporting Information

ABSTRACT: Cardamonin, a naturally occurring chalcone derivative, has demonstrated potential as a modulator of the endocannabinoid system (ECS). However, its interactions with cannabinoid receptors CB1 and CB2 are not fully understood. This work integrates in silico and in vivo methodology to examine the structural dynamics and pharmacological effects of cardamonin. Molecular dynamics simulations spanning 1000 ns demonstrated that cardamonin shows modest, receptor-dependent effects on CB1 dynamics, as shown by diminished root-mean-square deviation (RMSD) and fluctuation (RMSF), reduced solvent-accessible surface area (SASA), and increased hydrogen bonding. Principal component analysis (PCA) further demonstrated increased conformational sampling in CB1 following ligand binding, implying alteration of receptor flexibility. Conversely, CB2 had little structural alterations, indicating weaker or less selective binding. MM/PBSA binding energy calculations corroborated these findings, revealing that cardamonin exhibited comparable binding affinity at CB1 (−19.58 ± 6.49 kcal/mol) and CB2 (−18.76 ± 3.97 kcal/mol), with only a slight numerical tendency toward CB1. Both interactions were mild relative to the native ligands. Functional validation using Von Frey and Hargreaves behavioral experiments indicated that cardamonin markedly reduced mechanical and thermal hypersensitivity in mouse models. Significantly, some analgesic effects were maintained even with specific CB1 or CB2 blockade, suggesting receptor-biased or multitarget action. The robust alignment between computational predictions and behavioral evidence identifies cardamonin as a receptor-selective, physically stabilizing, and functionally significant modulator of CB1, with potential implications in nonopioid pain treatment approaches.

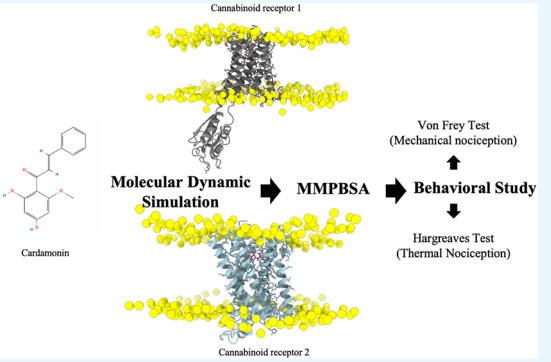

1. INTRODUCTION

Chronic pain is a significant and often difficult-to-manage condition affecting hundreds of millions of individuals globally. This condition is associated with various etiologies, such as inflammation, neuropathy, and tissue damage, and frequently coexists with anxiety, depression, and reduced quality of life. Despite progress in understanding pain neurobiology, current pharmaceutical strategies for pain management remain insufficient, often relying on opioids, nonsteroidal anti-inflammatory drugs (NSAIDs), antidepressants, and antiepileptics. These medications frequently exhibit limited long-term efficacy, adverse side effects, and a significant potential for dependency, particularly in the case of opioids.[1] This has created an urgent need to identify novel treatment targets and safer, more effective analgesic medications. The endocannabinoid system (ECS) functions as a key regulator of pain and inflammation. The ECS consists of endogenously synthesized lipid mediators, specifically anandamide and 2-arachidonoylglycerol, along with metabolic enzymes such as fatty acid amide hydrolase (FAAH) and monoacylglycerol lipase (MAGL). Additionally, it includes two main G protein-coupled receptors: cannabinoid receptor type 1 (CB1) and type 2 (CB2). CB1 is predominantly expressed in the brain and peripheral nervous system, where it plays a role in regulating neurotransmitter release, synaptic plasticity, and nociceptive transmission.[2,3] CB2 is predominantly found in immunological and hematopoietic cells, playing a role in the regulation of inflammation, cytokine secretion, and peripheral pain signaling.[4,5]

Both CB1 and CB2 receptors have been established as analgesic targets; however, the application of cannabinoid receptor ligands in clinical settings has faced significant

Received: October 1, 2025
Revised: January 27, 2026
Accepted: February 2, 2026
Published: April 13, 2026

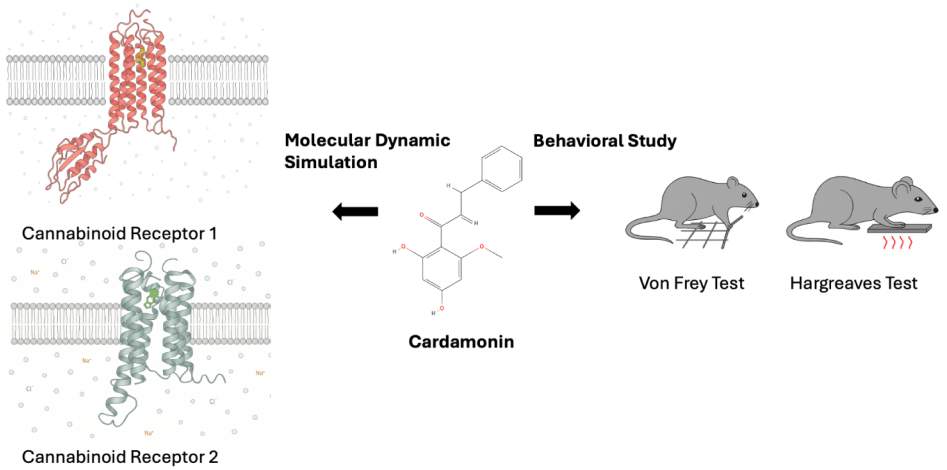

Figure 1. Schematic overview of the study design combining computational and behavioral approaches. Cardamonin, a chalcone derivative, was evaluated for its interaction with cannabinoid receptors CB1 and CB2 using molecular dynamics simulations and MM/PBSA analyses. Parallel in vivo behavioral assays—Von Frey and Hargreaves tests—were conducted in mice to assess mechanical and thermal antinociception, respectively.

obstacles. CB1 agonists effectively suppress pain and neuroinflammation; however, they are linked to central nervous system side effects, including psychotropic reactions, sedation, and tolerance.[6,7] CB2 agonists are characterized by peripheral restriction and enhanced safety, however, they frequently demonstrate low efficacy and receptor desensitization with chronic administration.[8] The therapeutic focus has shifted toward ligands that can partially activate or modulate CB receptors, avoiding overstimulation of canonical signaling pathways. This includes biassed agonists, allosteric modulators, and natural product-derived partial agonists.

Natural products constitute a significant and predominantly unexplored source of pharmacologically active compounds. In contrast to synthetic drugs that target a specific protein, numerous phytochemicals demonstrate polypharmacology by interacting with multiple signaling pathways to achieve therapeutic outcomes. The multitarget behavior is particularly significant in pain, as intricate interactions among the nervous system, immune response, and inflammation generate dynamic pathophysiological states. As a result, plant-derived secondary metabolites, especially flavonoids and chalcones, have garnered increasing attention as safe and effective scaffolds for drug discovery.[9] Cardamonin (2′,4′-dihydroxy-6′-methoxychalcone) is a naturally occurring chalcone derived from plants in the Zingiberaceae family, such as Alpinia katsumadai, Boesenbergia rotunda, and Alpinia conchigera. Cardamonin has been thoroughly investigated for its anti-inflammatory, antinociceptive, antioxidant, antiobesity, and anticancer effects.[10,11] It is recognized for its ability to inhibit NF-κB, MAPK, and JAK/STAT pathways, as well as to modulate cytokine release in immune and neuronal models.[10,12] Preclinical studies indicate that cardamonin reduces mechanical and thermal hypersensitivity in animal models of inflammatory pain; however, its molecular targets and mechanisms of receptor interaction are not yet defined. The lipophilic, planar structure of cardamonin, combined with its extensive anti-inflammatory properties, suggests a potential interaction with membrane-bound receptors that regulate nociception.

To date, the direct interaction of cardamonin with CB1 or CB2 receptors and its potential activity as a G protein-coupled receptors (GPCR) modulator have not been fully explored using advanced molecular approaches. This limits our mechanistic understanding of how natural products like cardamonin influence cannabinoid signaling and hampers their development as analgesic agents. In this study, we combined computational and experimental approaches to investigate cardamonin's receptor-binding properties and functional effects. We used structure-based molecular modeling and in vivo behavioral assays to show that cardamonin acts as a receptor-selective partial agonist or modulator, preferentially stabilizing CB1 through key polar contacts and conformational constraints. This stabilization is proposed to enhance antinociception in circuits dominated by CB1.

Molecular docking and long-time scale (1000 ns) molecular dynamics simulations were conducted to examine binding orientation, flexibility, and stability at CB1 and CB2 orthosteric sites (Figure 1). We analyzed metrics including RMSD, RMSF, solvent-accessible surface area, radius of gyration, hydrogen bond longevity, and principal component motions, and assessed relative binding energetics with MM/PBSA calculations. Computational predictions were tested in vivo using Von Frey and Hargreaves assays for pain sensitivity in mice, under both basal conditions and selective pharmacological blockade of CB1 and CB2 receptors (Figure 1). This integrative approach enabled clear attribution of cardamonin's analgesic effects to receptor interactions. In general, our results establish a mechanistic link between cardamonin's receptor-level actions and behavioral outcomes, supporting the potential of natural polyphenols as nonpsychotropic modulators of GPCR signaling in pain management.

2. MATERIALS AND METHODS

2.1. Molecular Docking Simulation

The three-dimensional crystal structures of human cannabinoid receptors CB1 (PDB ID: 5XR8)[13] and CB2[14] (PDB ID: 6PT0) were obtained from the RCSB Protein Data Bank (PDB) and prepared by removing all heteroatoms, water molecules, and cocrystallized ligands. Polar hydrogen atoms were added, and Gasteiger charges assigned using AutoDock Tools v1.5.6.[15] The 3D structure of cardamonin (PubChem CID: 5315675) was retrieved from the PubChem database and converted into PDBQT format via Open Babel.[16] Molecular docking simulations were conducted using AutoDock Vina,[17]

https://doi.org/10.1021/acsomega.5c10026
ACS Omega 2026, 11, 23820−23832

employing a stochastic global optimization algorithm to explore ligand conformational space within the orthosteric binding pocket. Grid boxes were defined to encompass the full ligand-binding domain to ensure optimal ligand accommodation and flexibility.Docking was performed using AutoDock Vina with a grid box centered at x = 0.24, y = 16.95, z = −64.81, and dimensions of 39.56 × 50.31 × 61.12 Å (size_x, size_y, size_z), ensuring full coverage of the ligand-binding region. The top-ranked pose, determined by the lowest predicted binding energy, was selected for subsequent molecular dynamics (MD) simulations. Protein−ligand interactions were analyzed and visualized using UCSF Chimera[18] and Discovery Studio Visualizer.

2.2. System Setup and Molecular Dynamics Simulations

Ligand-bound and control complexes for both CB1 and CB2 receptors were embedded into a palmitoyl-oleoyl-phosphatidylcholine (POPC) lipid bilayer using the CHARMM-GUI Membrane Builder.[19] Each system contained approximately 120−140 POPC lipids and was solvated with TIP3P water, providing ∼ 2.2 nm water thickness above and below the membrane. Sodium and chloride ions were added to neutralize the system at a physiological concentration of 0.15 M NaCl. Proteins and lipids were parametrized using the CHARMM36m force field,[20] while ligand parameters were assigned using CGenFF via the ParamChem server.[21] The ligand parameters for cardamonin were generated using the CGenFF 4.6 force field via the official ParamChem server, and all assigned penalties for bonded and nonbonded terms were below the recommended thresholds, indicating that cardamonin's chemical groups are well represented in the existing CGenFF parameter set and do not require QM-based reparameterization. To ensure robustness and rule out topology-related artifacts, all simulations were performed as three independent 1000 ns replicas for each system.

All MD simulations were performed using GROMACS 2022.2.[22] Following system construction, energy minimization was carried out using the steepest-descent algorithm with positional restraints. The steepest-descent method was chosen because it is robust for removing steric clashes and bad contacts in the early stages of system preparation, making it the standard initial minimization approach in GROMACS before equilibration. Equilibration followed the standard CHARMM-GUI six-step protocol, beginning with an NVT phase using the Berendsen thermostat (T = 310 K, τT = 1.0 ps), followed by semi-isotropic NPT equilibration using the Berendsen barostat (τP = 5.0 ps) and subsequently the Parrinello−Rahman barostat. During equilibration, position restraints were gradually released across steps 6.1−6.6. Production simulations were conducted for 1000 ns using a 2 fs time step with LINCS constraints applied to all bonds. Temperature was maintained at 310 K using the Nosé−Hoover thermostat (τT = 1.0 ps), and pressure was controlled at 1 atm using a semi-isotropic Parrinello−Rahman barostat (τP = 5.0 ps), allowing independent scaling of the membrane normal (z-axis) relative to the bilayer plane. Long-range electrostatics were treated using the Particle Mesh Ewald (PME) method, with a 1.2 nm cutoff for short-range Coulombic and van der Waals interactions. Neighbor lists were updated using the Verlet cutoff scheme. This simulation setup ensured stable membrane behavior, appropriate lateral lipid diffusion, and accurate sampling of GPCR dynamics over the extended trajectory.

2.3. Trajectory Analysis

Trajectory analysis was performed to evaluate the conformational stability and dynamics of CB1 and CB2 receptor complexes. RMSD (root-mean-square deviation) and RMSF (root-mean-square fluctuation) were calculated to assess backbone stability and residue-level flexibility, respectively. Radius of gyration (Rg) was analyzed to determine structural compactness, while solvent accessible surface area (SASA) was computed to assess changes in receptor surface exposure. The number of hydrogen bonds between cardamonin and the receptors was monitored across the trajectory to evaluate polar contact persistence. To assess large-scale conformational shifts, principal component analysis (PCA) was performed using the backbone covariance matrix and projection onto the top eigenvectors.[23−25] Simulation convergence was assessed using three independent 1000 ns replicas for each system, with analyses performed over the equilibrated 200−1000 ns window. RMSD, SASA, radius of gyration, and hydrogen-bond profiles showed stable, nondrifting behavior across all replicas, indicating that the systems had reached a converged equilibrium ensemble.

2.4. MM/PBSA Free Energy Calculation

MM/PBSA was selected as it provides an established and computationally efficient framework for estimating relative ligand binding free energies in large membrane-embedded GPCR systems. This approach is widely used in GPCR computational studies and offers a practical balance between accuracy and computational cost, whereas more rigorous alchemical free-energy methods (e.g., FEP/TI) would be prohibitively expensive for the present membrane−protein systems. Binding free energy calculations were carried out using the gmx_mmpbsa tool.[26] A total of 1000 snapshots extracted for each of 1 ns from each trajectory were used to compute average interaction energies. The total binding free energy was calculated as the sum of van der Waals, electrostatic, polar solvation, and nonpolar solvation contributions as shown in Equation (eq 1). These calculations provide insight into the relative stability and strength of cardamonin−receptor binding interactions. The uncertainties reported for all MM/PBSA energy components represent standard deviations, calculated from the distribution of GGAS and GSOLV values across the 1000 extracted snapshots. No confidence intervals were used. For the TOTAL free energy, the propagated uncertainty was computed using linear error propagation based on the standard deviations of the GGAS and GSOLV components.

$$\Delta G_{binding} = G_{complex} - (G_{receptor} + G_{ligand}) \quad (1)$$

2.5. Behavioral Experiments

2.5.1. Animals and Materials. The analgesic efficacy of Cardamonin (CDM) and its interaction with cannabinoid receptors (CB1 and CB2) were evaluated on chronic constriction injury (CCI) neuropathic pain animal model using two well-established behavioral tests in mice: the Von Frey test for mechanical allodynia and the Hargreaves test for thermal hyperalgesia. Both assays provide sensitive measures of pain response alterations following pharmacological interventions. All behavioral assays were conducted using n = 6 mice per group, which is consistent with established nociceptive testing guidelines and provides sufficient statistical power for

https://doi.org/10.1021/acsomega.5c10026
ACS Omega 2026, 11, 23820−23832

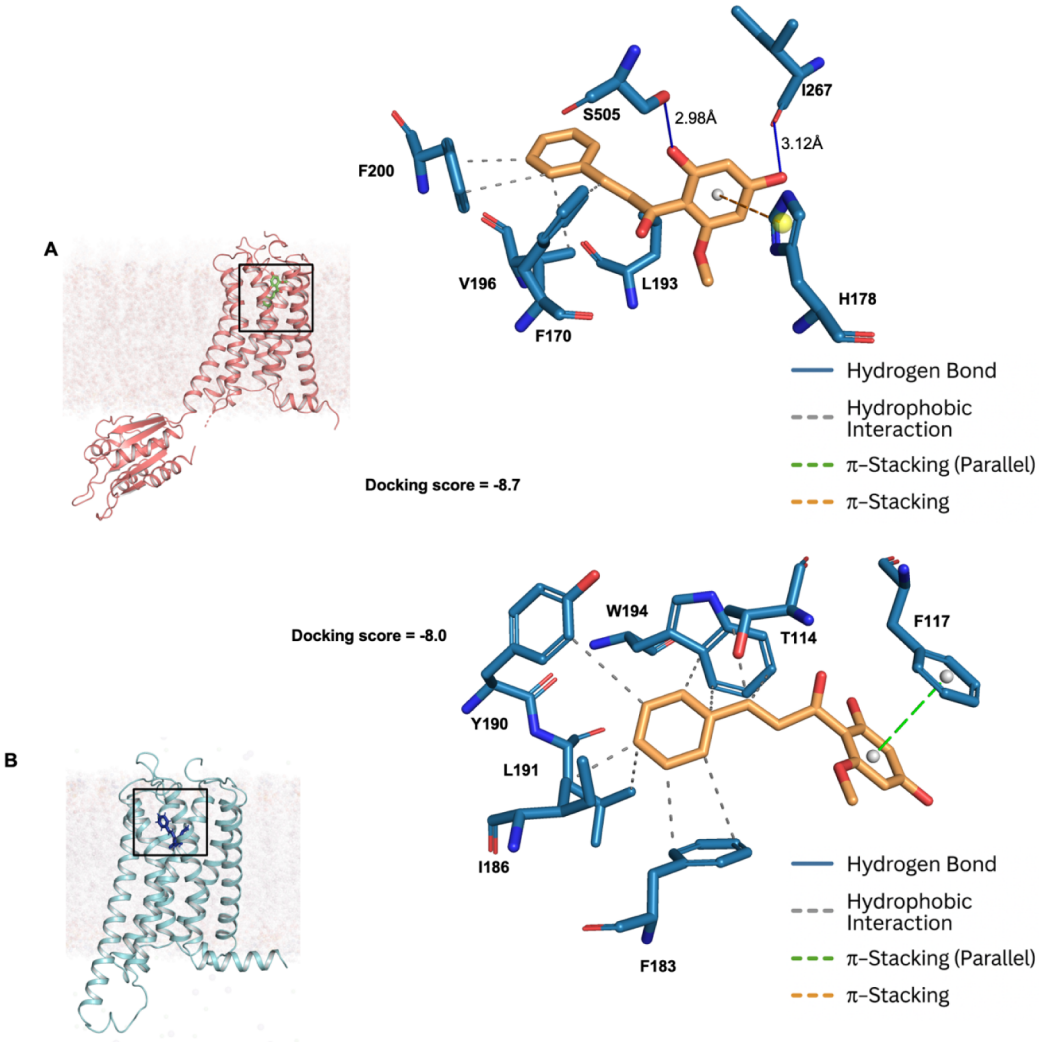

Figure 2. Docking poses of cardamonin with CB1 (A) and CB2 (B) receptors. (A) Cardamonin binds to CB1 with −8.7 kcal/mol, forming hydrogen bonds (SER_{505}, ILE_{267}), hydrophobic contacts (PHE_{170}, VAL_{196}, LEU_{193}, PHE_{200}), and a π-cation interaction (HIS_{178}). (B) In CB2 (−8.0 kcal/mol), cardamonin engages in hydrophobic interactions and a π-stacking (PHE117). Interaction types: hydrogen bonds (blue), hydrophobic (gray dashed), π-cation (orange dashed), π-stacking (green dashed).

ANOVA and posthoc analyses. A complete summary of all experimental groups is provided in Table S1.

Six to 8 weeks old male mice (25−30 g body weight) were housed under standard laboratory conditions (12-h light/dark cycle, controlled temperature, *ad libitum* access to food and water). All experimental protocols adhered to the ethical guidelines for laboratory animal care and use (Zimmermann, 1983) and were approved by the Institutional Animal Care and Use Committee (IACUC) with reference number UPM/IACUC/AUP-R033/2023. Cardamonin (MedChemExpress LLC, USA) and selective cannabinoid receptor 1 (CB1) antagonists SR141716 (MedChemExpress LLC, USA) and selective cannabinoid receptor 2 (CB2) antagonist SR144528 (MedChemExpress LLC, USA) were dissolved in dimethyl sulfoxide [DMSO], Tween 20 and diluted with saline at a ratio of 5:5:90 for intraperitoneal (i.p.) administration.

2.5.2. Behavioral Experiment Design. Mice were randomly assigned to sham-operated group, control groups consist of vehicle (DMSO)-treated group, CB1 antagonist (SR141716 1 mg/kg) group, CB2 antagonist (SR144528 1 mg/kg) group, and experimental groups consist of cardamonin (10 mg/kg)-treated group, CB1 antagonist pretreated and cardamonin-treated group, and CB2 antagonist pretreated and cardamonin-treated group. Mice were only used once throughout the experiments.

Mice were acclimatized to the laboratory environment, the apparatus chamber, and handling for 7 days prior to commencement of experiments. The selection of mice for the experiments and baseline data were recorded on day 0. Chronic constriction injury surgeries were performed on day 1 before mice were left to recover and exhibit neuropathic pain characteristics for 14 days. Treatments were given for 7 days starting from day 15 until day 21 and the mice were subsequently subjected to behavioral tests.

Chronic constriction injury (CCI) surgery was performed following the procedures outlined by Bennett and Xie (1988)[27] with slight modifications. Mice were first anaesthetized through intraperitoneal administration of 70 mg/kg sodium pentobarbital. After the mice were deeply anesthetized, fur at the surgical site was shaved to expose the skin, before povidone iodine was applied to disinfect the surgical area. One cm incision was made on right hind limb, parallel to femur. Muscle and skin layer are then separated by blunt dissection, before biceps femoris and gluteus superficialis muscles were separated

https://doi.org/10.1021/acsomega.5c10026
ACS Omega 2026, 11, 23820−23832

to expose the sciatic nerve. Four ligations with 1 mm distance are then made to sciatic nerve using 4−0 silk suture except for the sham-operated group. The skin was then sutured back using 4−0 nonabsorbable suture, before povidone iodine was applied.

Each experimental group included six animals and randomized to ensure statistical reliability. The researchers for the behavioral study and data analysis were blinded to the experimental treatments. Data were analyzed using standard statistical approaches, including one-way analysis of variance (ANOVA) followed by Tukey's posthoc test to compare between-group differences. Results were expressed as mean ± standard error of the mean (S.E.M), and statistical significance was defined as $p < 0.05$.

2.5.3. Von Frey Test for Mechanical Hyperalgesia. Mechanical nociceptive thresholds were assessed using dynamic plantar aesthesiometer (Ugo Basile, Italy). Briefly, mice were acclimatized individually in Plexiglas chambers on an elevated wire-mesh grid for approximately 30 min before testing. Von Frey filament was then placed perpendicularly below the plantar surface of right hind paw of the mice and pushed against the paw with an increasing force of 0.5 g to 5 g. The maximum force exerted were recorded once the mice withdrew its paw, with a cutoff point of 5 g force and 20s time to prevent tissue damage. A positive response was defined as a paw withdrawal reflex, licking, or flinching.

2.5.4. Hargreaves Test for Thermal Hyperalgesia. Thermal nociceptive thresholds were evaluated using the Hargreaves plantar test.[28] Mice were placed individually in Plexiglas chambers on an elevated glass platform and allowed to habituate for approximately 30 min. A radiant heat source (Hargreaves Apparatus, Ugo Basile, Italy) with fixed infrared intensity of 20 was positioned under the plantar surface of the right hind paw, and the latency time for paw withdrawal or licking was recorded automatically. To prevent tissue damage, a cutoff latency of 20 s was set. Care was taken to ensure no feces or urine stained on the glass before measurement was obtained for accuracy.

3. RESULTS AND DISCUSSION

3.1. Molecular Docking and Molecular Dynamics Analyses of Cardamonin with Cannabinoid Receptors

Docking simulations provided preliminary insights into the placement of cardamonin within the CB1 and CB2 receptor binding pockets, as illustrated in Figure 2. These docking poses represent the initial configurations used to initiate the MD simulations and are not intended to indicate dynamic stability. For CB1 (Figure 2A), cardamonin formed two hydrogen bonds with SER505 and ILE267 (2.98 Å and 3.12 Å). A π−cation interaction with HIS178 and hydrophobic contacts involving PHE170, VAL196, LEU193, and PHE200 contributed to the predicted docking pose. The docking score of −8.7 kcal/mol reflects a favorable orientation but should be interpreted qualitatively within the inherent uncertainties of docking scoring functions. For CB2 (Figure 2B), cardamonin formed a hydrogen bond with THR114, a π−π stacking interaction with PHE117, and hydrophobic contacts with ILE186, TYR190, LEU191, and TRP194. The docking score of −8.0 kcal/mol is only marginally different from CB1 and is not statistically meaningful. Accordingly, the docking results are used only to generate plausible starting poses, while receptor-selective trends are drawn from the subsequent MD simulations.

To further evaluate dynamic stability, MD simulations were conducted for 1000 ns on control and cardamonin-bound systems, as shown in Figure S1. Root mean square deviation (RMSD) analysis indicated stable global conformations for CB1, consistent with class A GPCRs.[29] To ensure replica-consistent interpretation, RMSD values were summarized across three independent replicas over the equilibrated 200−1000 ns window (Table S5), yielding pooled RMSD values of 1.161 ± 0.265 nm (control) and 1.043 ± 0.310 nm (cardamonin-bound).

In CB2, the control and cardamonin-bound systems showed comparable global stability; pooled RMSD values over 200−1000 ns were 0.265 ± 0.063 nm (control) and 0.325 ± 0.069 nm (cardamonin-bound) (Table S5), consistent with overlapping RMSD traces in Figure S1.

Root mean square fluctuation (RMSF) profiles, presented in Figure S2, showed broadly comparable residue-level fluctuations between the control and cardamonin-bound CB1 systems, with only modest local differences observed across transmembrane segments and extracellular loops. CB2 exhibited comparable but less pronounced reductions, supporting a weaker stabilizing effect.[30,31] These results suggest that cardamonin is associated with modest, localized differences in CB1 flexibility.[33]

Solvent-accessible surface area (SASA) analyses, illustrated in Figure S3, further demonstrated cardamonin's were used to examine potential ligand-associated changes in global solvent exposure. In CB1, pooled SASA values over the equilibrated 200−1000 ns window were 228.54 ± 5.98 nm^2 for the control system and 228.69 ± 5.13 nm^2 for the cardamonin-bound system (Table S5), indicating comparable solvent exposure within replica variability.[31] For CB2, pooled SASA values over 200−1000 ns were 167.91 ± 5.25 nm^2 (control) and 169.89 ± 5.04 nm^2 (cardamonin) (Table S5), likewise suggesting only minor differences within the overall variability.[34]

Consistent with these observations, the radius of gyration (Rg) analysis (Figure S4) was used as a global descriptor of compactness. Over the equilibrated 200−1000 ns window, pooled Rg values for CB1 were 2.990 ± 0.144 nm (control) and 3.024 ± 0.149 nm (cardamonin) (Table S5), indicating broadly comparable global compactness within replica variability. Similarly, CB2 showed pooled Rg values of 2.187 ± 0.038 nm (control) and 2.194 ± 0.037 nm (cardamonin) (Table S5), supporting minimal ligand-associated changes in overall compactness.

Overall, the docking and molecular dynamics simulations indicate that cardamonin remains stably associated with both CB1 and CB2 receptors over the simulated time scale without inducing large-scale structural rearrangements. Replica-averaged trajectory descriptors suggest modest, receptor-dependent differences in local dynamics for CB1, while CB2 remains largely unaffected. These observations remain within the range of typical GPCR behavior and do not support major functional state transitions based on molecular dynamics alone.

3.2. Hydrogen Bond Analysis

Hydrogen bond counts were computed for each frame of the 1000 ns MD trajectories of CB1 and CB2 in both native-ligand and cardamonin-bound states, as shown in Figure S5 and Table S5.

https://doi.org/10.1021/acsomega.5c10026
ACS Omega 2026, 11, 23820−23832

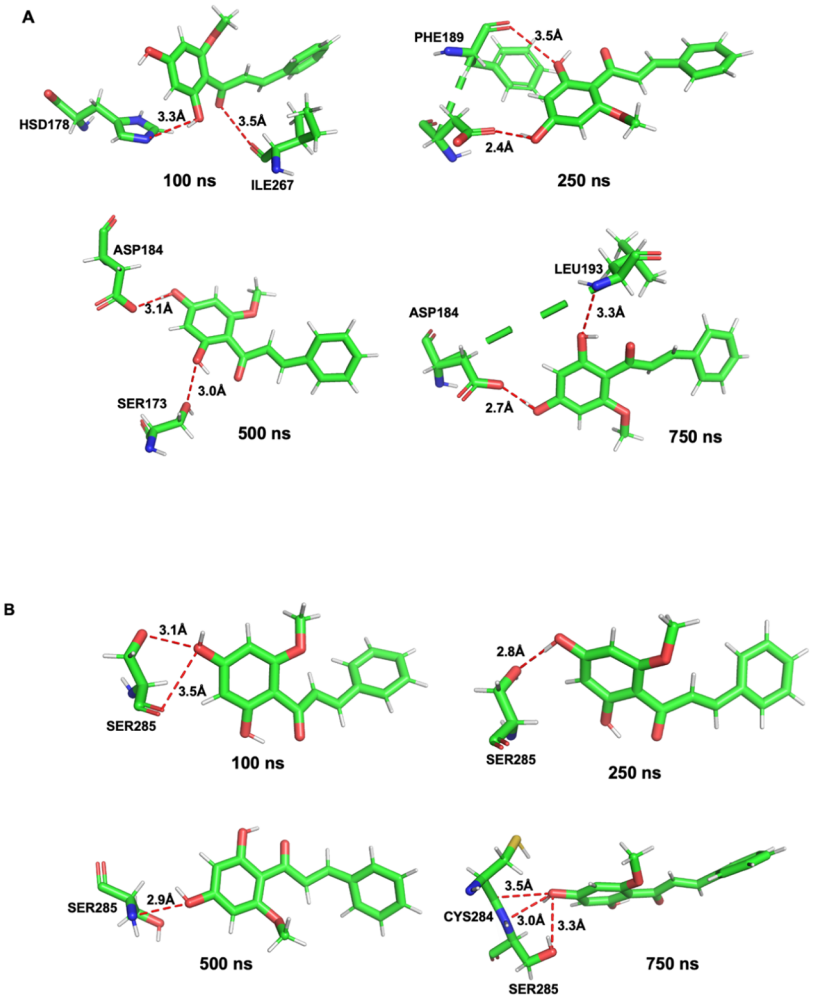

Figure 3. Hydrogen bond interaction snapshots between cardamonin and cannabinoid receptors CB1 (A) and CB2 (B) at selected time points from molecular dynamics simulations. Each frame corresponds to a representative structure at 100, 250, 500, and 750 ns. Hydrogen bonds are depicted as red dashed lines with annotated distances (Å). In CB1, dynamic repositioning of the ligand allows alternating interactions with residues such as HSD_{178}, ILE_{267}, PHE_{189}, ASP_{184}, SER_{173}, and LEU_{193}. In contrast, the CB2 complex demonstrates a more consistent hydrogen bonding profile, particularly with SER_{285} and GLY_{284}. These interactions reflect the temporal stability and flexibility of ligand−receptor engagement during the simulation trajectory.

In CB1, hydrogen bonds were observed throughout the trajectories, but replica-averaged analysis over the equilibrated 200−1000 ns window (Table S5) showed that the control (native ligand) system exhibited a higher pooled hydrogen-bond count (1.605 ± 0.588) than the cardamonin-bound system (0.867 ± 0.591). This indicates that cardamonin forms fewer and more transient polar contacts compared with the native ligand, rather than increasing hydrogen-bond persistence. These polar contacts likely involved residues in ECL2 and transmembrane helices, suggesting that cardamonin stabilizes key structural regions and enhances receptor rigidity. Hydrogen bonds in GPCRs can contribute to ligand anchoring and binding-site organization, although their persistence and frequency should be interpreted alongside other interaction types and global stability metrics.[31,34−36] Consistent with the RMSF and SASA analyses, hydrogen-bond counts alone do not indicate a strong ligand-driven rigidification, and therefore we interpret the hydrogen-bond results conservatively as reflecting transient polar contacts for cardamonin in CB1.

By contrast, CB2 exhibited overall low and intermittent hydrogen bond counts for both systems (Figure S5). Replica-averaged values over 200−1000 ns were 0.114 ± 0.318 (control) and 0.177 ± 0.397 (cardamonin) (Table S5), indicating that persistent hydrogen-bond networks are not a dominant interaction mode in CB2 within the simulated time scale.

Representative structural snapshots at 100, 250, 500, and 750 ns further illustrate these differences as illustrated in Figure 3. In CB1, cardamonin established dynamic hydrogen bonds with residues including HSD_{178}, ILE_{267}, PHE_{189}, ASP_{184}, SER_{173}, and LEU_{193}, showing temporal adaptability while maintaining persistent engagement. In CB2, interactions were more confined, consistently involving SER_{285} and occasionally GLY_{284}, but lacking the same temporal flexibility. These snapshots illustrate representative polar contacts observed during the simulations; however, comparative interpretations between CB1 and CB2 are based primarily on the quantitative, replica-averaged MD metrics (Table S5) and MM/PBSA binding energies rather than on individual frames. These residue-level interactions describe the types of contacts observed during the simulation; however, the representative snapshots are provided for visualization only and are not used alone to infer receptor stability. Comparative interpretations

https://doi.org/10.1021/acsomega.5c10026
ACS Omega 2026, 11, 23820−23832

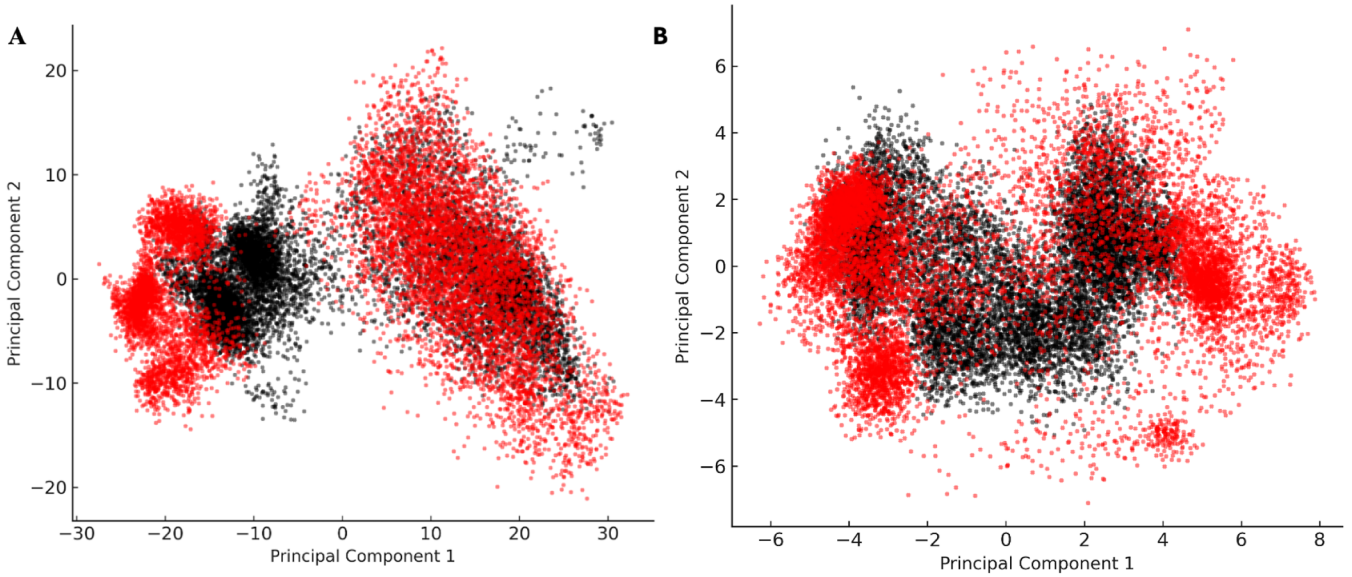

Figure 4. Principal Component Analysis (PCA) of CB1 and CB2 receptor complexes. (A) PCA projection of CB1 control (black) and cardamonin-bound complex (red) onto the first two principal components. Cardamonin binding induces broader conformational sampling. (B) PCA projection of CB2 control (black) and cardamonin-bound complex (red), showing overlapping conformational space and reduced ligand impact.

between CB1 and CB2 rely instead on the quantitative, replica-averaged MD metrics and MM/PBSA binding energies.

3.3. Principal Component Analysis (PCA)

Principal component analysis (PCA) was performed to quantify the dominant collective motions of CB1 and CB2 over the 1000 ns simulations. PCA reduces the high-dimensional MD trajectories into orthogonal principal components (PCs) derived from the covariance matrix of atomic positional fluctuations, allowing visualization of the most prominent slow, large-amplitude motions. PCA projections were evaluated across all three independent replicas using the equilibrated 200−1000 ns window, and replica-wise as well as pooled PC1−PC2 summary statistics (mean ± SD and dispersion) are provided in Table S6. In GPCRs, these components often reflect subtle rearrangements of transmembrane helices, loop flexibility, and global breathing motions that contribute to conformational sampling. Here, trajectory frames for the control and cardamonin-bound complexes were projected onto the first two principal components (PC1 and PC2), which captured the largest fraction of conformational variance (Figure 4). For CB1, both the control and ligand-bound ensembles occupied partially overlapping regions of the PC1−PC2 space. The cardamonin-bound system sampled a slightly broader distribution along PC1, suggesting modest increases in the range of accessible global motions, but the overlap between the two states indicates that the dominant conformational modes remain largely similar. No well-separated clusters or distinct conformational basins were observed, implying that cardamonin does not induce major transitions into alternative global structural states within the simulated time scale. This interpretation is consistent with the replica-averaged trajectory descriptors (RMSD/RMSF) indicating stable global conformations with only modest differences between control and cardamonin-bound systems.

For CB2, the PCA projections of the control and ligand-bound complexes showed extensive overlap with nearly identical dispersion patterns along both principal components. This close correspondence indicates that cardamonin binding results in minimal changes to the large-scale motions of CB2, consistent with the small differences observed in the RMSF and hydrogen-bond analyses. The limited separation between control and ligand-bound states suggests that CB2 dynamics remain largely unaltered during the simulation. Overall, PCA indicates that cardamonin does not produce major global rearrangements in either receptor. Both CB1 and CB2 maintain similar dominant motion patterns, with only small ligand-associated variations that fall within typical GPCR dynamic behavior. Because these differences are subtle, no mechanistic conclusions regarding receptor activation, desensitization, or biased signaling were inferred from the PCA results.

3.4. MM/PBSA Binding Free Energy Analysis

The Molecular Mechanics/Poisson−Boltzmann Surface Area (MM/PBSA) method was employed to assess the binding free energies of cardamonin to cannabinoid receptors CB1 and CB2. MM/PBSA is a recognized postprocessing method for estimating ligand−receptor affinities in molecular dynamics simulations, integrating molecular mechanics energies with solvation models to approximate the Gibbs free energy of binding.[26,37] This approach divides the total binding energy into four primary components: van der Waals (VDWAALS), electrostatic (EEL), polar solvation (EPB), and nonpolar solvation (ENPOLAR). The components elucidate the relative contributions of hydrophobic, polar, and electrostatic forces in the stabilization of ligand−protein complexes.

The CB1 control system exhibited a total binding free energy of − 42.47 ± 5.06 kcal/mol, driven primarily by favorable van der Waals (−59.01 ± 2.54 kcal/mol) and electrostatic (−18.38 ± 3.65 kcal/mol) interactions. Polar solvation contributions (EPB: + 40.35 ± 3.18 kcal/mol) partially offset these favorable terms due to desolvation penalties. The cardamonin-bound CB1 complex showed a total binding free energy of −19.58 ± 6.49 kcal/mol, reflecting

https://doi.org/10.1021/acsomega.5c10026
ACS Omega 2026, 11, 23820−23832

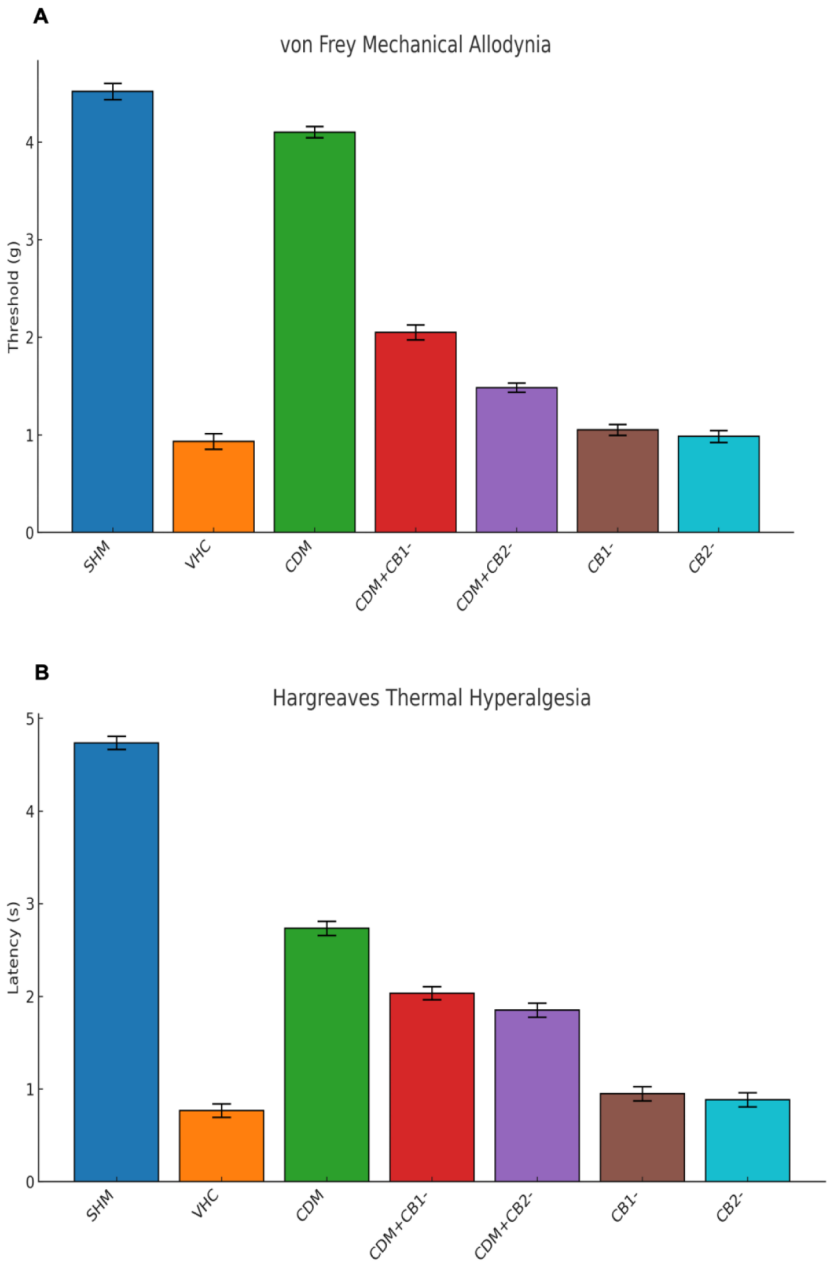

Figure 5. (A) Mechanical paw withdrawal threshold (mean ± SEM) in the Von Frey test. SHM and CDM groups displayed high thresholds (normal sensitivity), while VHC, CB1$^-$, and CB2$^-$ groups exhibited mechanical allodynia. Co-treatment with cardamonin (CDM+CB1$^-$ and CDM +CB2$^-$) partially restored pain thresholds. (B) Thermal paw withdrawal latency (mean ± SEM) in the Hargreaves test. SHM group showed normal latency. CB1$^-$, CB2$^-$, and VHC groups exhibited thermal hyperalgesia. Cardamonin (CDM) increased latency significantly, and cotreatment with CB1$^-$ or CB2$^-$ partially restored thermal sensitivity.

reduced stabilizing interactions relative to the control. This decrease is consistent with lower van der Waals (−37.21 ± 2.88 kcal/mol) and electrostatic (−10.56 ± 4.39 kcal/mol) components, suggesting weaker intermolecular complementarity within the CB1 orthosteric pocket. These trends align with MD observations showing limited hydrogen bonding and moderate structural modulation in RMSD, RMSF, SASA, and PCA analyses.

A similar pattern was observed for CB2. The control system displayed a binding free energy of −37.05 ± 5.20 kcal/mol, dominated by van der Waals contributions (−60.00 ± 2.94 kcal/mol). The cardamonin-bound CB2 complex showed a total free energy of −18.76 ± 3.97 kcal/mol, again indicating reduced stabilizing interactions relative to the native ligand. Although the difference between control and ligand-bound CB2 is somewhat smaller than in CB1, the overall trend likewise reflects weaker interaction strength, consistent with the minimal perturbations detected in RMSD, RMSF, and PCA profiles.

Overall, the MM/PBSA decomposition indicates that cardamonin binds more weakly to both CB1 and CB2 compared with their respective native ligands, supporting the qualitative observation of reduced intermolecular stabilization in the MD trajectories. These results complement the broader structural analyses and highlight modest, receptor-dependent differences in cardamonin interaction strength. Even if the total binding free energies of the CB1 and CB2 complexes differ numerically, their tiny discrepancy (0.8 kcal/mol) is well

https://doi.org/10.1021/acsomega.5c10026
ACS Omega 2026, 11, 23820−23832

within the propagated uncertainty of the MM/PBSA approach (4−6 kcal/mol). Therefore, rather than being regarded as quantitative evidence of preferential affinity toward a single receptor, these findings should be understood qualitatively, as evidence of generally reduced stabilization following cardamonin binding. Uncertainties in the TOTAL binding free energies were recalculated using linear propagation of errors from the GGAS and GSOLV components to ensure consistency with standard statistical treatment.

The difference between docking and MM/PBSA binding energies is expected, as the two methods rely on fundamentally different scoring principles. Docking provides approximate, pose-based scores from static structures, whereas MM/PBSA incorporates solvent effects and averages energies across MD snapshots. Therefore, their magnitudes are not directly comparable, and the comparison should be interpreted qualitatively rather than quantitatively.

3.5. Von Frey Test and Hargreaves Test

The Von Frey test was performed to assess mechanical nociceptive thresholds in mice after treatment with cardamonin, selective cannabinoid receptor antagonists ($CB1^-$ and $CB2^-$), and their combinations (Figure 5). This assay utilizes calibrated monofilaments on the plantar surface to assess paw withdrawal thresholds, commonly employed to quantify mechanical allodynia and antinociceptive efficacy in rodent pain models.[38,39] Statistical analysis (ANOVA summary, Table S2) showed significant group differences ($p < 0.05$), and Tukey's post hoc comparisons (Table S3) confirmed significant pairwise differences. Mice in the sham group (SHM) demonstrated normal thresholds (4.52 ± 0.08 g), indicating preserved mechanical sensitivity. Cardamonin alone (CDM) did not significantly affect the baseline (4.10 ± 0.06 g), indicating that it does not induce mechanical hypersensitivity in healthy animals. Mice treated with vehicle (VHC), along with those pretreated with $CB1^-$ and $CB2^-$ antagonists, exhibited significantly lower thresholds (0.93 ± 0.08 g, 1.05 ± 0.06 g, and 0.98 ± 0.06 g, respectively), suggesting the presence of mechanical allodynia after cannabinoid receptor blockade. This aligns with the recognized function of CB1 and CB2 in sustaining antinociceptive tone through the ECS.[40,41]

The coadministration of cardamonin with antagonists resulted in a partial restoration of nociceptive thresholds. The CDM+$CB1^-$ group demonstrated a significant increase of 2.05 ± 0.08 g, whereas the CDM+$CB2^-$ group exhibited a moderate rise of 1.48 ± 0.05 g. The results suggest that cardamonin maintains partial antinociceptive activity despite receptor blockade, although it does not return to baseline levels. The mechanical sensitivity data indicate that cardamonin alleviates allodynia induced by CB1/CB2 blockade, exhibiting more pronounced effects when CB1 is inhibited. This suggests an increased dependence on CB2 signaling for mechanical antinociception, consistent with previous research emphasizing CB2's involvement in peripheral pain modulation and the resolution of inflammation.[42] The findings collectively indicate the receptor-selective analgesic potential of cardamonin and suggest the involvement of additional pathways beyond CB1/CB2, potentially including anti-inflammatory or TRP channel-related mechanisms.[40]

3.6. Hargreaves Test: Thermal Nociceptive Response

The Hargreaves test was utilized to evaluate thermal sensitivity in mice, providing insights into heat-induced nociceptive responses after cannabinoid receptor modulation shown in Figure 5B. The assessment evaluates paw withdrawal latency in reaction to a standardized infrared stimulus, where reduced latencies signify hyperalgesia.[28] Thermal nociceptive thresholds were significantly different across groups (ANOVA, Table S2), with detailed post hoc differences summarized in Table S4. The sham group (SHM) exhibited the highest latency (4.73 ± 0.07 s), indicating typical thermal nociception. In contrast, the vehicle-treated (VHC), $CB1^-$, and $CB2^-$ groups demonstrated significantly reduced latencies (0.77 ± 0.07 s, 0.95 ± 0.08 s, and 0.88 ± 0.07 s, respectively), thereby confirming the occurrence of thermal hyperalgesia induced by cannabinoid receptor blockade. Mice administered cardamonin (CDM) exhibited an increased withdrawal latency of 2.73 ± 0.08 s, demonstrating a significant thermal analgesic effect. This indicates that cardamonin may activate thermal antinociceptive mechanisms without relying on injury-induced sensitization. The coadministration of receptor antagonists partially reversed hyperalgesia, with CDM+$CB1^-$ yielding 2.03 ± 0.07 s and CDM+$CB2^-$ resulting in 1.85 ± 0.08 s. The effects, although diminished in comparison to CDM alone, showed significant enhancement when contrasted with antagonist-only groups. The observed partial restoration of latency with both antagonists indicates that cardamonin's thermal antinociceptive effects engage both CB1 and CB2 receptors, albeit not exclusively. The increased latency observed in CDM+$CB1^-$ indicates a greater dependence on CB2 for thermal pain suppression, which contrasts with the Von Frey results that suggested a predominant role of CB1 in mechanical allodynia. The behavioral outcomes support the analgesic potential of cardamonin through both CB receptor-dependent and receptor-independent mechanisms. This duality may facilitate the treatment of mixed-pain phenotypes prevalent in chronic inflammatory and neuropathic disorders. Post hoc statistical analysis (Tukey's HSD) confirmed significant differences among treatment groups in both the mechanical (Von Frey) and thermal (Hargreaves) nociceptive assays.

3.7. Integration of Molecular Dynamics and Behavioral Outcomes

This study combines MD simulations and behavioral tests to investigate cardamonin's effects on CB1 and CB2 receptors. By integrating structural and energetic data with in vivo pain assays, we developed a clear and receptor-specific model explaining cardamonin's mechanism of action.

Contrary to initial expectations that cardamonin might destabilize CB1 upon binding, RMSD analysis (Figure S1A) indicated that the cardamonin-bound CB1 complex exhibited a more stable profile than the control system. The RMSD curve demonstrated a diminished fluctuation range and attained equilibrium sooner, indicating that cardamonin plays a role in local receptor stabilization. RMSF data (Figure S2A) further substantiated this observation, indicating reduced atomic fluctuations, especially in transmembrane helices and extracellular loops adjacent to the ligand-binding domain. This stabilization suggests that cardamonin may enhance structural rigidity in critical regions while preserving overall conformational flexibility.[32] The SASA analysis (Figure S3A) revealed a modest decrease in solvent-accessible surface area for the cardamonin-bound CB1 complex, suggesting a more compact receptor conformation. This compaction is frequently linked to stabilization induced by binding. Analysis of hydrogen bonds (Figure S5A) indicated the establishment of consistent and

https://doi.org/10.1021/acsomega.5c10026
ACS Omega 2026, 11, 23820−23832

Table 1. MM/PBSA Binding Free Energy Decomposition for CB1 and CB2 Receptors with and without Cardamonin.[a]

	CB1 + Cardamonin	CB1 Control	CB2 + Cardamonin	CB2 Control
VDWAALS	-37.21 ± 2.88	-59.01 ± 2.54	-38.69 ± 2.04	-60.00 ± 2.94
EEL	-10.56 ± 4.39	-18.38 ± 3.65	-5.29 ± 2.62	-9.01 ± 3.27
EPB	31.90 ± 4.05	40.35 ± 3.18	28.85 ± 2.29	36.97 ± 2.23
ENPOLAR	-3.70 ± 0.10	-5.43 ± 0.09	-3.62 ± 0.09	-5.01 ± 0.09
GGAS	-47.77 ± 5.09	-77.39 ± 3.93	-43.99 ± 3.24	-69.00 ± 4.70
GSOLV	28.19 ± 4.03	34.92 ± 3.19	25.23 ± 2.29	31.95 ± 2.22
TOTAL	−19.58 ± 6.49 kcal/mol	−42.47 ± 5.06 kcal/mol	-−18.76 ± 3.97 kcal/mol	−37.05 ± 5.20 kcal/mol

[a]This table presents the energy components derived from MM/PBSA calculations, including van der Waals (VDWAALS), electrostatic (EEL), polar solvation (EPB), and nonpolar solvation (ENPOLAR) energies. The gas phase energy (GGAS) and solvation energy (GSOLV) contribute to the final binding free energy (TOTAL).

recurring hydrogen bonds during the simulation, implying robust polar interactions with critical residues. Stable interactions may improve the structural integrity of the binding pocket and support an inactive or intermediate receptor conformation.[30,31,36] The data indicate that cardamonin does not destabilize CB1; instead, it appears to stabilize the receptor through polar interactions and compaction of the transmembrane core, potentially affecting receptor signaling states. In contrast to its effects on CB1, Cardamonin demonstrated negligible structural influence on CB2. The RMSD (Figure S1B), RMSF (Figure S2B), and SASA (Figure S3B) values for the cardamonin-bound CB2 complex closely aligned with those of the control, indicating a minimal conformational response to ligand binding. Hydrogen bonding (Figure S5B) was infrequent and temporary, exhibiting occasional peaks during the initial stages of simulation but lacking prolonged interaction. The results suggest a diminished or less specific binding mode in CB2, possibly attributable to reduced complementarity between cardamonin and the receptor's binding pocket, or variations in receptor dynamics that promote transient ligand interactions. This aligns with CB2's more adaptable architecture and may account for the reduced binding affinity noted.

Principal Component Analysis (PCA, Figure 4) provided a more profound understanding of the global dynamics influenced by cardamonin binding. PCA projections for CB1 indicated an increase in the conformational sampling space of the ligand-bound receptor relative to the control. The wider distribution of principal components 1 and 2 signifies increased mobility among metastable states, indicating that cardamonin influences the receptor's global motions, potentially driving it toward inactive or intermediate functional states. In contrast, CB2 exhibited minimal variation between the control and cardamonin-bound states. The PCA clusters exhibited significant overlap, indicating that cardamonin does not induce considerable global conformational changes in CB2. This suggests that its binding is less functionally disruptive and potentially less effective within the CB2 context. PCA data further support the notion that cardamonin preferentially modulates CB1 over CB2, both in structural and dynamic aspects.

To confirm the differential interactions identified in trajectory and PCA analyses, MM/PBSA binding free energy calculations were conducted (Table 1). Cardamonin demonstrated comparable total binding energy for CB1 (−19.58 ± 6.49 kcal/mol) compared to CB2 (−18.76 ± 3.97 kcal/mol), but tendency toward CB1, indicating a higher affinity for CB1. The affinities, although moderate relative to their native ligands (−42.47 kcal/mol for CB1-control and − 37.05 kcal/mol for CB2-control), are adequate to facilitate functional engagement.[30,43] The energy decomposition analysis indicated that van der Waals interactions were the primary contributors to cardamonin binding in both receptors. CB1 exhibited a more favorable balance of electrostatic and solvation components, characterized by enhanced polar desolvation, indicating a tighter integration within its hydrophobic pocket. The energetic insights correspond with the trajectory data, reinforcing a model in which cardamonin preferentially stabilizes CB1 through noncovalent interactions.

This study's in vivo component demonstrated physiological evidence supporting the analgesic potential of cardamonin. The behavioral outcomes from the Von Frey and Hargreaves assays closely aligned with the in-silico findings, providing translational support for the computational predictions. In the Von Frey assay, mice pretreated with $CB1^{-}$, $CB2^{-}$ antagonists, or vehicle (VHC) exhibited significantly reduced paw withdrawal thresholds, indicating the presence of mechanical allodynia. The administration of cardamonin restored thresholds to nearly normal levels, thereby confirming its antinociceptive efficacy. The cotreatment groups (CDM $+CB1^{-}$ and CDM+$CB2^{-}$) demonstrated a partial reversal of hypersensitivity, with elevated thresholds relative to the antagonist-only groups, yet still lower than those observed with cardamonin alone. This indicates that cardamonin maintains functional activity despite partial blockade of CB1 or CB2, suggesting either dual-receptor engagement or noncanonical mechanisms of action. In the Hargreaves assay, both vehicle- and antagonist-treated animals displayed hyperalgesia, indicated by reduced paw withdrawal latencies, whereas cardamonin treatment notably extended withdrawal times. Co-treatment groups exhibited intermediate effects, indicating a partial dependence on CB1/CB2 signaling pathways. The consistent results observed in both assays indicate that cardamonin exhibits broad-spectrum antinociceptive effects, which are partially mediated by the modulation of cannabinoid receptors.

The alignment between MD simulations and behavioral observations supports several cautious but meaningful interpretations. Cardamonin shows slightly more persistent hydrogen-bonding and modest structural compaction in CB1 than in CB2, although these differences are subtle and fall within the range of comparable receptor dynamics. Accordingly, the behavioral findings should be viewed as consistent with minor CB1-leaning trends, rather than indicating strong or preferential selectivity.

- Energetic Perspective: MM/PBSA calculations show that the binding free energies for CB1 and CB2 are highly similar, with only small numerical differences that

https://doi.org/10.1021/acsomega.5c10026
ACS Omega 2026, 11, 23820−23832

lie within the uncertainty range. This indicates that cardamonin acts as a moderate-affinity ligand for both receptors, aligning more closely with a partial modulator than a high-affinity agonist.

- Dynamic Modulation: PCA analysis reveals subtle, nondisruptive changes in the conformational sampling of CB1 upon cardamonin binding, while CB2 exhibits nearly overlapping motion profiles between apo and bound states. These modest differences may reflect minor local adjustments rather than distinct activation pathways.
- Receptor Independence: The persistence of analgesic effects even in the presence of CB1 or CB2 antagonists suggests that cardamonin's antinociceptive activity is not solely dependent on classical cannabinoid receptor signaling. Its overall behavioral profile may also be influenced by other processes, such as allosteric effects, secondary target engagement, or downstream signaling cascade regulation.

The findings indicate that cardamonin does not function as a classical orthosteric cannabinoid agonist. It operates via dynamic receptor modulation, selectively influencing the structural and energetic landscape of CB1, while also partially engaging CB2 or other targets. This multimodal mechanism may enhance the analgesic efficacy observed in vivo, positioning Cardamonin as a promising lead compound for pain management with minimal psychoactive liability. Although the compound demonstrates mechanistic promise and preliminary antinociceptive activity, its safety, metabolic stability, and tolerability remain to be established. Future work should include comprehensive ADME/Tox profiling to evaluate its suitability as a therapeutic candidate.

4. CONCLUSIONS

Cardamonin, a natural chalcone, selectively stabilizes the CB1 receptor over CB2, as revealed by MD simulations, energetic analyses, and behavioral experiments. The ligand promotes inactive or intermediate CB1 states, broadening its conformational landscape and reducing pain sensitivity without adverse psychoactive or desensitizing effects. Compared with CB2, cardamonin shows greater binding affinity and functional impact at CB1, even when CB1/CB2 antagonists are present, indicating a receptor-specific, modulatory mechanism. These findings support the potential of cardamonin as a promising noneuphoric, plant-derived analgesic and multitarget pain modulator via selective GPCR conformational reprogramming

■ ASSOCIATED CONTENT

Data Availability Statement

All molecular dynamics (MD) and MM/PBSA input files used in this study are publicly available in the following GitHub repository: https://github.com/arifjamali-90/Receptor-Selective-Modulation-of-Cannabinoid-Signaling-by-Cardamonin.

Supporting Information

The Supporting Information is available free of charge at https://pubs.acs.org/doi/10.1021/acsomega.5c10026.

Additional figures and tables describing molecular docking results, replica-averaged molecular dynamics analyses (RMSD, RMSF, SASA, Rg), hydrogen bond analysis, principal component analysis, and MM/PBSA free energy calculations are provided in the Supporting Information (PDF)

■ AUTHOR INFORMATION

Corresponding Author

Muhamad Arif Mohamad Jamali − *Faculty of Science and Technology, Universiti Sains Islam Malaysia, Bandar Baru Nilai, Negeri Sembilan 71800, Malaysia;* orcid.org/0000-0002-1642-3062; Email: arifjamali@usim.edu.my

Authors

Mohamed Hanief Khalid − *Faculty of Medicine and Health Sciences, Universiti Sains Islam Malaysia, Bandar Baru Nilai, Negeri Sembilan 71800, Malaysia; Department of Biomedical Science, Faculty of Medicine and Health Sciences, Universiti Putra Malaysia, Serdang, Selangor 43400, Malaysia*

Liyana Azmi − *Faculty of Medicine and Health Sciences, Universiti Sains Islam Malaysia, Bandar Baru Nilai, Negeri Sembilan 71800, Malaysia*

M. Qadri E. Mubarak − *Faculty of Science and Technology, Universiti Sains Islam Malaysia, Bandar Baru Nilai, Negeri Sembilan 71800, Malaysia;* orcid.org/0000-0001-8384-7984

Nur Mazniatul Iqma Marsujak − *Department of Biomedical Science, Faculty of Medicine and Health Sciences, Universiti Putra Malaysia, Serdang, Selangor 43400, Malaysia*

Amir Syahir − *Nanobiotechnology Research Group, Department of Biochemistry, Faculty of Biotechnology and Biomolecular Sciences, Universiti Putra Malaysia, Serdang, Selangor 43400, Malaysia;* orcid.org/0000-0002-3305-7957

Enoch Kumar Perimal − *Curtin Medical School, Faculty of Health Sciences, Curtin University, Bentley, WA 6102, Australia*

Mohd Roslan Sulaiman − *Department of Biomedical Science, Faculty of Medicine and Health Sciences, Universiti Putra Malaysia, Serdang, Selangor 43400, Malaysia*

Complete contact information is available at: https://pubs.acs.org/10.1021/acsomega.5c10026

Author Contributions

#M.H.K., L.A., and M.Q.E.M. equally contributed. Conceptualization: M.H.K., E.K.P., M.A.M.J.; Data Curation: M.H.K., N.M.I.M., M.A.M.J., M.Q.E.M.; Formal analysis: M.H.K., L.A., M.A.M.J., M.Q.E.M.; Funding acquisition: M.R.S., M.A.M.J., A.S.; Investigation: M.H.K., N.M.I.M., M.A.M.J.; Methodology: M.H.K., E.K.P., M.A.M.J.; Visualization: L.A., M.A.M.J., M.Q.E.M.; Writing − original draft: M.H.K., M.A.M.J., N.M.I.M., M.Q.E.M.; Writing − review and editing: L.A., M.Q.E.M., A.S., E.K.P., M.R.S. The manuscript was written through substantial contributions of all authors. All authors have given approval to the final version of the manuscript.

Funding

This research was funded by Universiti Sains Islam Malaysia under the USIM Research Grant with reference code PPPI/USIM/FST/USIM/112523, and Geran Putra Berimpak (GP-GPB/2022/9711700) from Universiti Putra Malaysia.

Notes

The authors declare no competing financial interest.

■ ACKNOWLEDGMENTS

MAMJ thanks all the authors for their valuable discussions during the preparation of this manuscript.

■ REFERENCES

(1) Volkow, N. D.; Michaelides, M.; Baler, R. The Neuroscience of Drug Reward and Addiction. *Physiol Rev.* **2019**, *99*, 2115−2140.
(2) Mackie, K. Cannabinoid Receptors as Therapeutic Targets. *Annu. Rev. Pharmacol. Toxicol.* **2006**, *46*, 101.
(3) Howlett, A. C. The Cannabinoid Receptors. *Prostaglandins Other Lipid Mediat.* **2002**, *68*−*69*, 619−631.
(4) Turcotte, C.; Blanchet, M. R.; Laviolette, M.; Flamand, N. The CB2 Receptor and Its Role as a Regulator of Inflammation. *Cell. Mol. Life Sci.* **2016**, *73*, 4449.
(5) Zou, S.; Kumar, U. Cannabinoid Receptors and the Endocannabinoid System: Signaling and Function in the Central Nervous System. *Int. J. Mole. Sci.* **2018**, *19*, 833.
(6) Pertwee, R. G. The Diverse CB1 and CB2 Receptor Pharmacology of Three Plant Cannabinoids: Delta9-Tetrahydrocannabinol, Cannabidiol and Delta9-Tetrahydrocannabivarin. *Br. J. Pharmacol.* **2008**, *153*, 199−215.
(7) Atwood, B. K.; MacKie, K. CB 2: A Cannabinoid Receptor with an Identity Crisis. *Br. J. Pharmacol.* **2010**, *160*, 467.
(8) Morales, P.; Hernandez-Folgado, L.; Goya, P.; Jagerovic, N. Cannabinoid Receptor 2 (CB2) Agonists and Antagonists: A Patent Update. *Expert Opin. Ther. Pat.* **2016**, *26*, 843.
(9) Pan, S. Y.; Zhou, S. F.; Gao, S. H.; Yu, Z. L.; Zhang, S. F.; Tang, M. K.; Sun, J. N.; Ma, D. L.; Han, Y. F.; Fong, W. F.; Ko, K. M. New Perspectives On How To Discover Drugs From Herbal Medicines: cam's Outstanding Contribution To Modern Therapeutics. *Evidence Based Complementary Altern. Med.* **2013**, *2013*, 627375.
(10) Daimary, U. D.; Parama, D.; Rana, V.; Banik, K.; Kumar, A.; Harsha, C.; Kunnumakkara, A. B. Emerging Roles of Cardamonin, a Multitargeted Nutraceutical in the Prevention and Treatment of Chronic Diseases. *Curr. Res. Pharmacol. Drug Discovery* **2021**, *2*, 100008.
(11) Barber, K.; Mendonca, P.; Evans, J. A.; Soliman, K. F. A. Antioxidant and Anti-Inflammatory Mechanisms of Cardamonin through Nrf2 Activation and NF-KB Suppression in LPS-Activated BV-2 Microglial Cells. *Int. J. Mol. Sci.* **2023**, *24*, 10872.
(12) Lee, J. -H.; Jung, H. S.; Giang, P. M.; Jin, X.; Lee, S.; Son, P. H.; Lee, D.; Hong, Y. -S.; Lee, K.; Jung, J. J. Blockade of Nuclear Factor-KB Signaling Pathway and Anti-Inflammatory Activity of Cardamomin, a Chalcone Analog from Alpinia Conchigera. *J. Pharmacol. Exp. Ther.* **2006**, *316*, 271−278.
(13) Hua, T.; Vemuri, K.; Pu, M.; Qu, L.; Han, G. W.; Wu, Y.; Zhao, S.; Shui, W.; Li, S.; Korde, A.; et al. Crystal Structure of the Human Cannabinoid Receptor CB1. *Cell* **2016**, *167*, 754−758.
(14) Xing, C.; Zhuang, Y.; Xu, T.H.; Feng, Z.; Zhou, X.E.; Chen, M.; Wang, L.; Meng, X.; Xue, Y.; Wang, J.; et al. Structural Basis of Ligand Recognition and G-Protein Coupling of the Cannabinoid Receptor CB2. *Cell* **2020**, *180*, 645−654.e13.
(15) Morris, G. M.; Ruth, H.; Lindstrom, W.; Sanner, M. F.; Belew, R. K.; Goodsell, D. S.; Olson, A. J. Software News and Updates AutoDock4 and AutoDockTools4: Automated Docking with Selective Receptor Flexibility. *J. Comput. Chem.* **2009**, *30*, 2785−2791.
(16) O'Boyle, N. M.; Banck, M.; James, C. A.; Morley, C.; Vandermeersch, T.; Hutchison, G. R. Open Babel: An Open Chemical Toolbox. *J. Cheminform.* **2011**, *3*, 10.
(17) Trott, O.; Olson, A. J. AutoDock Vina: Improving the Speed and Accuracy of Docking with a New Scoring Function, Efficient Optimization, and Multithreading. *J. Comput. Chem.* **2010**, *31*, 455−461.
(18) Pettersen, E. F.; Goddard, T. D.; Huang, C. C.; Couch, G. S.; Greenblatt, D. M.; Meng, E. C.; Ferrin, T. E. UCSF Chimera - A Visualization System for Exploratory Research and Analysis. *J. Comput. Chem.* **2004**, *25*, 1605−1612.
(19) Jo, S.; Kim, T.; Iyer, V. G.; Im, W. CHARMM-GUI: A Web-Based Graphical User Interface for CHARMM. *J. Comput. Chem.* **2008**, *29*, 1859−1865.
(20) Huang, J.; Rauscher, S.; Nawrocki, G.; Ran, T.; Feig, M.; De Groot, B. L.; Grubmüller, H.; MacKerell, A. D. CHARMM36m: An Improved Force Field for Folded and Intrinsically Disordered Proteins. *Nat. Methods* **2016**, *14*, 71−73.
(21) Vanommeslaeghe, K.; Hatcher, E.; Acharya, C.; Kundu, S.; Zhong, S.; Shim, J.; Darian, E.; Guvench, O.; Lopes, P.; Vorobyov, I.; et al. CHARMM General Force Field: A Force Field for Drug-like Molecules Compatible with the CHARMM All-Atom Additive Biological Force Fields. *J. Comput. Chem.* **2010**, *31*, 671−690.
(22) Abraham, M. J.; Murtola, T.; Schulz, R.; Páll, S.; Smith, J. C.; Hess, B.; Lindah, E. Gromacs: High Performance Molecular Simulations through Multi-Level Parallelism from Laptops to Supercomputers. *SoftwareX* **2015**, *1*−*2*, 19−25.
(23) Amadei, A.; Linssen, A. B. M.; Berendsen, H. J. C. Essential Dynamics of Proteins. *Proteins: struct., Funct., Bioinf.* **1993**, *17*, 412−425.
(24) David, C. C.; Jacobs, D. J. Principal Component Analysis: A Method for Determining the Essential Dynamics of Proteins. In *Protein Dynamics*; Springer, 2014, Vol. *1084*, pp. 193-226. DOI: .
(25) Hollingsworth, S. A.; Dror, R. O. Molecular Dynamics Simulation for All. *Neuron* **2018**, *99*, 1129.
(26) Kumari, R.; Kumar, R.; Consortium, O. S. D. D.; Lynn, A. G _ Mmpbsa - A GROMACS Tool for MM-PBSA and Its Optimization for High-Throughput Binding Energy Calculations. *J. Chem. Inf. Model.* **2014**, *54*, 1951−1962.
(27) Bennett, G. J.; Xie, Y. -K. A Peripheral Mononeuropathy in Rat That Produces Disorders of Pain Sensation like Those Seen in Man. *Pain* **1988**, *33*, 87−107.
(28) Hargreaves, K.; Dubner, R.; Brown, F.; Flores, C.; Joris, J. A New and Sensitive Method for Measuring Thermal Nociception in Cutaneous Hyperalgesia. *Pain* **1988**, *32*, 77−88.
(29) Dror, R. O.; Pan, A. C.; Arlow, D. H.; Borhani, D. W.; Maragakis, P.; Shan, Y.; Xu, H.; Shaw, D. E. Pathway and Mechanism of Drug Binding to G-Protein-Coupled Receptors. *Proc. Natl. Acad. Sci. U. S. A.* **2011**, *108*, 13118−13123.
(30) Miao, Y.; McCammon, J. A. G-Protein Coupled Receptors: Advances in Simulation and Drug Discovery. *Curr. Opin. Struct. Biol.* **2016**, *41*, 83.
(31) Manglik, A.; Kim, T. H.; Masureel, M.; Altenbach, C.; Yang, Z.; Hilger, D.; Lerch, M. T.; Kobilka, T. S.; Thian, F. S.; Hubbell, W. L.; et al. Structural Insights into the Dynamic Process of B2-Adrenergic Receptor Signaling. *Cell* **2015**, *161*, 1101−1111.
(32) Latorraca, N. R.; Venkatakrishnan, A. J.; Dror, R. O. GPCR Dynamics: Structures in Motion. *Chem. Rev.* **2017**, *117*, 139.
(33) Venkatakrishnan, A. J.; Deupi, X.; Lebon, G.; Tate, C. G.; Schertler, G. F.; Babu, M. M. Molecular Signatures of G-Protein-Coupled Receptors. *Nature* **2013**, *494*, 185−194.
(34) Katritch, V.; Cherezov, V.; Stevens, R. C. Structure-Function of the G Protein-Coupled Receptor Superfamily. *Annu. Rev. Pharmacol. Toxicol.* **2013**, *53*, 531.
(35) Miao, Y.; McCammon, J. A. Unconstrained Enhanced Sampling for Free Energy Calculations of Biomolecules: A Review. *Mol. Simul.* **2016**, *42*, 1046−1055.
(36) Hubbard, R. E.; Haider, M. K. Hydrogen Bonds in Proteins: Role and Strength. *Encycl. Life Sci.* **2010**.
(37) Genheden, S.; Ryde, U. The MM/PBSA and MM/GBSA Methods to Estimate Ligand-Binding Affinities. *Expert Opin. Drug Discovery* **2015**, *10*, 449.
(38) Chaplan, S. R.; Bach, F. W.; Pogrel, J. W.; Chung, J. M.; Yaksh, T. L. Quantitative Assessment of Tactile Allodynia in the Rat Paw. *J. Neurosci. Methods* **1994**, *53*, 55−63.
(39) Pitcher, G. M.; Ritchie, J.; Henry, J. L. Paw Withdrawal Threshold in the Von Frey Hair Test Is Influenced by the Surface on Which the Rat Stands. *J. Neurosci. Methods* **1999**, *87*, 185−193.
(40) Pertwee, R. G. Pharmacology of Cannabinoid Receptor Ligands. *Curr. Med. Chem.* **2022**, *6*, 635−664.

https://doi.org/10.1021/acsomega.5c10026
ACS Omega 2026, 11, 23820−23832

(41) Rahn, E. J.; Hohmann, A. G. Cannabinoids as Pharmacotherapies for Neuropathic Pain: From the Bench to the Bedside. *Neurotherapeutics* **2009**, *6*, 713−737.
(42) Ibrahim, M. M.; Porreca, F.; Lai, J.; Albrecht, P. J.; Rice, F. L.; Khodorova, A.; Davar, G.; Makriyannis, A.; Vanderah, T. W.; Mata, H. P.; et al. CB2 Cannabinoid Receptor Activation Produces Antinociception by Stimulating Peripheral Release of Endogenous Opioids. *Proc. Natl. Acad. Sci. U. S. A.* **2005**, *102*, 3093−3098.
(43) Gertsch, J.; Pertwee, R. G.; Di Marzo, V. Phytocannabinoids beyond the Cannabis Plant - Do They Exist? *Br. J. Pharmacol.* **2010**, *160*, 523.

https://doi.org/10.1021/acsomega.5c10026
ACS Omega 2026, 11, 23820−23832